Composite Photonic Crystals from Semiconductor Nanocrystal/Polyelectrolyte-Coated Colloidal Spheres

Dayang Wang,[†] Andrey L. Rogach,[‡] and Frank Caruso*[,§]

Max Planck Institute of Colloids and Interfaces, D-14424 Potsdam, Germany, Photonics and Optoelectronics Group, Physics Department and CeNS, University of Munich, D-80799 Munich, Germany, and Department of Chemical and Biomolecular Engineering, The University of Melbourne, Victoria 3010, Australia

Received January 8, 2003. Revised Manuscript Received April 14, 2003

Submicrometer-sized polystyrene colloidal spheres were coated with hybrid films consisting of HgTe semiconductor nanocrystal (HgTe NC) and polyelectrolyte (PE) multilayers by the layer-by-layer (LbL) technique. The prepared coated spheres were crystallized, forming composite colloidal crystals. Increasing the number of the HgTe NC layers deposited on the colloidal spheres leads to an increase in both the diameter and the effective refractive index of the spheres, which causes a systematic red shift of the stop bands of the composite colloidal crystals. The photoluminescence properties of the HgTe NCs assembled around the spheres in the composite colloidal crystals are impacted by the stop band of the colloidal crystals, giving rise to modifications of their emission properties. A titanium(IV) isopropoxide (TIP)/isopropyl alcohol solution was infiltrated into the voids of the colloidal crystals, and after solidification of TIP and removal of the colloidal crystal template by calcination, composite TiO_2/HgTe inverse opals with HgTe embedded in the interior surface of the macroporous TiO_2 were obtained. The strategy presented demonstrates the feasibility of fabricating composite photonic crystals (both colloidal crystals and inverse opals) from nanoscale-coated colloidal spheres. Such composite opaline photonic crystals provide a means of combining electronic confinement, originating from the NCs, with photon confinement, due to the ordered dielectric structures, hence opening new avenues in the design and construction of novel electrooptical devices based on photonic crystals.

Introduction

Three-dimensional (3D) ordered dielectric structures with lattice parameters comparable to the wavelength of electromagnetic waves are attracting considerable interest, mainly because of their possible applications as 3D photonic band gap (PBG) crystals.[1] Photonic crystals exhibit a PBG, an energy range for which light cannot propagate in any direction inside the crystal, giving them the unique properties of localizing light and controlling spontaneous emission. These ordered materials are of interest in diverse applications, ranging from optics to optoelectronics, and even to optical computers.[2] Structures with a PBG in the optical (infrared[3a] and near-infrared[3b]) region have been fabricated by lithographic "stacking" techniques. As the structures are further scaled down to below infrared wavelengths, the aligning of subsequent layers to form ordered 3D materials becomes difficult, and sample yields decrease as additional layers are stacked. The fabrication procedures currently available also make this process tedious and expensive.

Self-assembly of monodisperse colloidal spheres provides an alternative and versatile route for the fabrication of optical photonic crystals.[4] Monodisperse colloidal spheres (e.g., silica or polymer) are known to spontaneously self-organize into several crystal structures (face-centered-cubic, fcc, or body-centered-cubic, bcc) with long-range periodicity. An inverted structure of colloidal crystals, or inverse opal, is a 3D macroporous structure that comprises highly ordered air spheres interconnected to each other by small channels.[5] These macroporous structures can be produced by infilling the voids between the spheres making up the colloidal crystals

* To whom correspondence should be addressed. Tel.: +61 3 8344 3461. Fax: +61 3 8344 4153. E-mail: fcaruso@unimelb.edu.au.
[†] Max Planck Institute of Colloids and Interfaces.
[‡] University of Munich.
[§] The University of Melbourne.

(1) (a) Joannopoulos, J. D.; Meade, R. D.; Winn, J. N. *Photonic Crystals, Molding the Flow of Light*; Princeton University Press: Singapore, 1997. (b) Krauss, T. F.; De La Rue, R. M. *Prog. Quantum Electron.* **1999**, *23*, 51. (c) Berger, V. *Curr. Opin. Solid State Mater. Sci.* **1999**, *4*, 209.

(2) (a) Yablonovitch, E. *Phys. Rev. Lett.* **1987**, *58*, 2059. (b) John, S. *Phys. Rev. Lett.* **1987**, *58*, 2086.

(3) (a) Lin, S.; Fleming, J. G.; Hetherington, D. L.; Smith, B. K.; Biswas, R.; Ho, K. M.; Sigalas, M. M.; Zubrzycki, W.; Kurtz, S. R.; Bur, J. *Nature* **1998**, *394*, 251. (b) Noda, S.; Tomoda, K.; Yamamoto, N.; Chutinan, A. *Science* **2000**, *289*, 604.

(4) See, for example: (a) Ozin, G. A.; Yang, S. M. *Adv. Funct. Mater.* **2001**, *11*, 95. (b) Velev, O. D.; Lenhoff, A. M.; Kaler, E. W. *Science* **2000**, *287*, 2240. (c) Jiang, P.; Bertone, J. F.; Hwang, K. S.; Colvin, V. L. *Chem. Mater.* **1999**, *11*, 2132. (d) van Blaaderen, A.; Ruel, R.; Wiltzius, P. *Nature* **1997**, *385*, 321. (e) Asher, S. A.; Holtz, J.; Weissman, J.; Pan, G. *MRS Bull.* **1998**, *11*, 44. (f) Mayoral, R.; Requena, J.; Moya, J. S.; Lopez, C.; Cintas, A.; Miguez, H.; Mesaguer, F.l; Vazquez, L.; Holgado M.; Blanco, A. *Adv. Mater.* **1997**, *9*, 257.

(5) (a) Stein, A.; Schroden, R. C. *Curr. Opin. Solid State Mater. Sci.* **2001**, *5*, 553. (b) Stein, A. *Microporous Mesoporous Mater.* **2001**, *44*−*45*, 227. (c) Norris, D. J.; Vlasov, Y. A. *Adv. Mater.* **2001**, *13*, 371. (d) Velev, O. D.; Lenhoff, A. M. *Curr. Opin. Colloid Interface Sci.* **2000**, *5*, 56. (e) Xia, Y.; Gates, B.; Yin, Y.; Liu, Y. *Adv. Mater.* **2000**, *12*, 693.

10.1021/cm031003o CCC: $25.00
Published on Web 06/19/2003

with other materials and by removing the colloidal crystal templates by calcination or etching. By using approaches such as sol−gel chemistry, electrodeposition, and chemical vapor deposition and a variety of colloidal crystals as templates, inverse opals with a range of compositions have been prepared, including metals,[6] metal oxides,[7] semiconductors,[8,9] carbon,[10] and polymers.[11]

The formation of an absolute (i.e., complete) PBG in the visible and near-infrared wavelength range requires a high refractive index contrast (>2.8) for simple structures (fcc or bcc) and negligible absorption. The wavelength of the absorption edge of the materials, however, is proportional to the fourth power of the refractive index,[8a] so few materials (e.g., silicon) satisfy this requirement to form an absolute PBG in the near-infrared range.[9] Although most colloidal crystals or inverse opals with simple structures (fcc or bcc) do not produce an absolute PBG in the visible and near-infrared wavelength range (often because of low refractive index contrasts), they show optical stop bands along certain crystal directions (i.e., they only exhibit a pseudo band gap). This property can, however, be exploited to modify the spontaneous emission of organic dyes,[12] rare-earth ions and their organic complexes,[13] and semiconductor nanocrystals (NCs)[14] embedded in the voids of colloidal crystals.

Semiconductor NCs with sizes comparable to the electron de Broglie wavelength (1−10 nm) exhibit size-tunable electronic and optical properties due to 3D electronic confinement.[15] Doping of PBG crystals with luminescent semiconductor NCs permits the realization of the combination of electronic and photonic confinement, which might enable one to engineer the electron and photon densities of states separately within one structure. This would provide a potentially powerful means to create novel light sources with controllable spontaneous emission. To date, semiconductor NCs have been introduced into the voids between spheres of silica colloidal crystals using chemical vapor[8c−d,9,14a] and electro- or chemical bath deposition,[8b,14b,c] as well as colloid chemical techniques.[8a,14d−e]

In the current work, we report an alternative and flexible approach for forming composite photonic crystal structures. We employ colloidal spheres coated with a hybrid shell of semiconductor NCs and polyelectrolytes (PEs) as the building blocks for fabricating colloidal crystals. The spheres were prepared by the layer-by-layer assembly technique,[16] which is based on the electrostatic interaction between oppositely charged species deposited onto colloidal spheres.[17] This approach provides a facile way to form core−shell particles with nanoscale control over the coating thickness and composition, and final particle diameter. Colloidal crystals are formed from polystyrene (PS) spheres coated with HgTe NC/PE multilayers of different thicknesses. The influence of the number of HgTe NC layers on the optical properties of the colloidal crystals is investigated. The photoluminescence characteristics of the HgTe NCs in the composite colloidal crystals are also examined. Additionally, TiO_2/HgTe composite inverse opals are prepared by using the colloidal crystals of the HgTe NC/PE multilayer-coated colloidal spheres as templates. The current work builds on our preliminary study, where we demonstrated the crystallization of coated colloidal spheres comprising polystyrene cores and CdTe NCs embedded in a preassembled three-layer-thick PE film.[18]

Experimental Section

Materials. Poly(allylamine hydrochloride) (PAH), M_w 8000−11 000, and poly(sodium 4-styrensulfonate) (PSS), M_w 70 000, were obtained from Aldrich. PSS was dialyzed against Milli-Q water (M_w cutoff 14 000) and lyophilized before use. Details on the synthesis of the negatively charged HgTe NCs (3.5 nm diameter, 13 mmol L^{-1} with reference to Hg) capped by thioglycerol can be found elsewhere.[19] Negatively charged sulfate-stabilized polystyrene (PS) spheres of diameter 640 nm were prepared as described earlier.[20] Sodium chloride (NaCl), isopropyl alcohol (IPA), and titanium(IV) isopropoxide (TIP) were purchased from Aldrich. The water used in all experiments was from a three-stage Millipore Milli-Q Plus 185 purification system and had a resistivity higher than 18.2 MΩ cm.

(6) (a) Kulinowski, K. M.; Jiang, P.; Vaswani, H.; Colvin, V. L. *Adv. Mater.* **2000**, *12*, 833. (b) Egaan, G. L.; Yu, J. S.; Kim, C. H.; Lee, S. J.; Shaak, R. E.; Mallouk, T. E. *Adv. Mater.* **2000**, *12*, 1040. (c) Xu, L.; Zhou, W. L.; Frommen, C.; Baoughman, R. H.; Zakhidov. A. A.; Malkinski, L.; Wang, J.; Wiley, J. B. *Chem. Commun.* **2000**, 997. (d) Yan, H.; Blanford, C. F.; Holland, B. T.; Parent, M.; Smyrl, W. H.; Stein, A. *Adv. Mater.* **1999**, *11*, 1003.

(7) (a) Turner, M. E.; Trentler, T. J.; Colvin, V. L. *Adv. Mater.* **2001**, *13*, 180. (b) Holland, B. T.; Blanford, C. F.; Stein, A. *Science* **1998**, *281*, 538. (c) Holland, B. T.; Blanford, C. F.; Do, T.; Stein, A. *Chem. Mater.* **1999**, *11*, 795. (d) Imhof, A.; Pine, D. J. *Nature* **1997**, *389*, 948.

(8) (a) Vlasov, Y. A.; Yao, N.; Norris, D. J. *Adv. Mater.* **1999**, *11*, 165. (b) Braun, P. V.; Wiltzius, P. *Adv. Mater.* **2001**, *13*, 482. (c) Míguez, H.; Chomski, E.; García-Santamaría, F.; Ibisate, M.; John, S.; López, C.; Meseguer, F.; Mondia, J. P.; Ozin, G. A.; Toader, O.; van Driel H. M.; *Adv. Mater.* **2001**, *13*, 634. (d) Müller, M.; Zentel, R.; Maka, T.; Romanov, S.; Sotomayor Torres, C. M. *Adv. Mater.* **2000**, *12*, 1499.

(9) (a) Vlasov, Y. A.; Bo, X. Z.; Norris, J. C. *Nature* **2001**, *414*, 289. (b) Blanco, A.; Chomski, E.; Grabtchak, S.; Ibisate, M.; John, S.; Leonard, S. W.; Lopez, C.; Meseguer, F.; Miguez, H.; Mondia, J. P.; Ozin, G. A.; Toader, O.; van Driel, H. M. *Nature* **2000**, *405*, 437.

(10) Zakhidov, A. A.; Baughman, R. H.; Iqbal, Z.; Cui, C. X.; Khayrullin, I.; Dantas, S. O.; Marti, I.; Ralchenko, V. G. *Science* **1998**, *282*, 897.

(11) (a) Gates, B.; Yin, Y.; Xia, Y. *Chem. Mater.* **1999**, *11*, 2827. (b) Johnson, S. A.; Olivier, P. J.; Mallouk, T. E. *Science* **1999**, *283*, 963. (c) Jiang, P.; Cizeron, J.; Bertone, J. F.; Colvin, V. L. *J. Am. Chem. Soc.* **1999**, *121*, 11630. (d) Cassagneau, T.; Caruso, F. *Adv. Mater.* **2002**, *14*, 34. (e) Wang, D.; Caruso, F. *Adv. Mater.* **2001**, *13*, 353. (f) Deutsch, M.; Vlasov, Y. A.; Norris, D. J. *Adv. Mater.* **2000**, *12*, 1176.

(12) (a) Petrov, E. P.; Bogomolov, V. N.; Kalosha, I. I.; Gaponenko, S. V. *Phys. Rev. Lett.* **1998**, *81*, 77. (b) Yamasaki, T.; Tsutsui, T. *Appl. Phys. Lett.* **1998**, *72*, 1957. (c) Yoshino, K.; Tada, K.; Ozaki, M.; Zakhidov, A. A.; Baughman, R. H. *Appl. Phys. Lett.* **1998**, *73*, 3506.

(13) Gaponenko, S. V.; Bogomolov, V. N.; Petrov, E. P.; Kapitonov, A. M.; Yarotsky, D. A.; Kalosha, I. I.; Eychmueller, A. A.; Rogach, A. L.; McGilp, J.; Woggon, U.; Gindele, F. *J. Lightwave Technol.* **1999**, *17*, 2128.

(14) (a) Vlasov, Yu. A.; Luterova, K.; Pelant, I.; Hönerlage, B. Astratov, V. N. *Appl. Phys. Lett.* **1997**, *71*, 1616. (b) Blanco, A.; Lopez, C.; Mayoral, R.; Meseguer, F.; Mifsud, A.; Herrero, J. *Appl. Phys. Lett.* **1998**, *73*, 1781. (c) Romanov, S. G.; Fokin, A. V.; Alperovich, V. I.; Johnson, N. P.; De La Rue, R. M. *Phys. Status Solidi A* **1997**, *164*, 169. (d) Gaponenko, S. V.; Kapitonov, A. M.; Bogomolov, V. N.; Prokofiev, A. V.; Eychmüller, A.; Rogach, A. L. *JETP Lett.* **1998**, *68*, 142. (e) Rogach, A.; Ostrander, J.; Nagesha, D.; Giersig, M.; Kotov, N. *Chem. Mater.* **2000**, *12*, 2676.

(15) (a) Alivisatos, A. P. *Science* **1996**, *277*, 933. (b) Weller, H. *Adv. Mater.* **1993**, *5*, 88.

(16) (a) Decher, G.; Hong, J. D. *Makromol. Chem. Macromol. Symp.* **1991**, *46*, 321. (b) Decher, G. *Science* **1997**, *277*, 1232.

(17) (a) Caruso, F.; Caruso, R. A.; Möhwald, H. *Science* **1998**, *282*, 1111. (b) Donath, E.; Sukhorukov, G. B.; Caruso, F.; Davis, S. A.; Möhwald, H. *Angew. Chem., Int. Ed.* **1998**, *37*, 2201. (c) Caruso, F. *Adv. Mater.* **2001**, *13*, 11.

(18) Rogach, A.; Susha, A.; Caruso, F.; Sukhorukov, G.; Kornowshi, A.; Kershaw, S.; Möhwald, H.; Eychmüller, A.; Weller, H. *Adv. Mater.* **2000**, *12*, 333.

(19) Rogach, A.; Kershaw, S. V.; Burt, M.; Harrison, M.; Kornowski, A.; Eychmüller, A.; Weller, H. *Adv. Mater.* **1999**, *11*, 552.

(20) Furusawa, K.; Norde, W.; Lyklema, J. *Kolloid Z. Z Polym.* **1972**, *250*, 908.

Coating of PS Spheres with HgTe NC/PE Multilayers. Prior to the deposition of the HgTe NC layers, a "primer" three-layer PE film was formed by the alternate adsorption of PAH and PSS (1 mL from 1 mg mL^{-1} solutions containing 0.5 M NaCl) onto 0.2 mL of negatively charged PS spheres (1 wt %, $\sim 10^{10}$ spheres), as described earlier.[21] The PE adsorption time was 20 min. After each adsorption step, excess PE was removed by four repeated centrifugation (5000*g* for 10 min)/wash/redispersion cycles. The three-layer PE-coated PS spheres had a positively charged surface, as determined by microelectrophoresis experiments.[21]

The HgTe NC coatings on the PS spheres were formed by the addition 0.8 mL of an aqueous NC solution to 0.2 mL of the PE-coated PS colloidal dispersion, allowing 60 min for NC adsorption, removing excess NCs by four repeated centrifugation (5000*g* for 10 min)/wash/redispersion cycles, and subsequently depositing PAH/PSS/PAH (1 mL from 1 mg mL^{-1} solutions containing 0.5 M NaCl), as outlined above for the primer layers. This process was repeated until the desired number of NC/PE layers was formed. To form colloidal crystal films on quartz slides, an additional PAH/PSS double layer was deposited on the HgTe NC/PE multilayer-coated spheres, as this facilitated formation of the crystals (see later). The resulting coated spheres are denoted as PS−$(PE_3$/HgTe NC$)_n$/PE_2, where *n* is the number of the PE_3/HgTe NC layers.

Fabrication of Composite Colloidal Crystals from Coated Spheres. Colloidal crystals of the coated spheres were formed on quartz slides using a method similar to that introduced by Nagayama et al.[22] The cell for crystallization of the particles consisted of a 2-cm-thick poly(tetrafluoroethylene) (Teflon) block with a 1-cm-diameter opening running through the middle. This block was placed on the quartz slide, and the slide and Teflon block were then clamped between two steel plates having a 1-cm circular opening [positioned directly over the opening in the poly(tetrafluoroethylene) block]. Forty microliters of the PS−$(PE_3$/HgTe NC$)_n$/PAH/PSS colloidal dispersion was placed in the chamber, and after water evaporation, colloidal crystal films of 1 cm in diameter were obtained.

Synthesis of TiO_2/HgTe Inverse Opals. An IPA solution of TIP was used as supplied to form TiO_2. The volume ratio of TIP to IPA in the solution was about 1:10. The IPA/TIP solution was pipetted onto the PS−$(PE_3$/HgTe NC$)_n$/PAH/PSS colloidal crystal film on the quartz slide [no poly(tetrafluoroethylene) block present]; another quartz slide was immediately placed on top of the colloidal crystal film; and two clips were used to tightly fix these two slides, with the colloidal crystal film sandwiched between the two slides. The samples were then dried under ambient conditions. The soaking and drying cycle was repeated 5 times to ensure that the voids between the colloidal spheres in the templates were sufficiently filled. After removal of the material (PS spheres and PE multilayers) by calcination (heating to 500 °C at a rate of 5 °C min^{-1} under nitrogen and then at 500 °C for 1−2 h under oxygen), TiO_2/HgTe composite inverse opal films were formed on quartz slides.

Characterization. Scanning electron microscopy (SEM) measurements and energy-dispersive X-ray (EDX) spectra were collected with a JEOL/JSM-63330F field-emission scanning electron microscope operated at 5 kV. SEM samples were placed on carbon surfaces and then sputter-coated with Au (~5 nm thick). Transmission electron microscopy (TEM) measurements were undertaken with a Philips CM12 microscope operating at 120 kV. The reflection spectra were recorded with an infrared spectrophotometer (Bruker IFS66) in the near-infrared range at an angle of incidence of 12°. Photoluminescence (PL) spectra of the PS−$(PE_3$/HgTe NC$)_2$/PE_2 colloidal crystals were collected by exciting them with an argon ion laser ($\lambda = 514$ nm) and detecting the PL with a cooled Ge photodiode (North Coast EO 817L).

Results and Discussion

Composite Colloidal Crystals of PS−$(PE_3$/NC$)_n$/PE_2 Spheres. HgTe NCs that display strong emission in the near-infrared range have been synthesized as aqueous dispersions.[19] Previous work has shown that, using the electrostatic interaction between negatively charged HgTe NCs and positively charged polyelectrolytes, HgTe NC/PE nanocomposite multilayer films can be built up on planar surfaces.[23] In the current work, to fabricate uniform HgTe NCs films on PS spheres, PE multilayers (PAH/PSS/PAH, PE_3) were deposited on the spheres prior to deposition of the HgTe NCs. The PE multilayers provide a smooth and uniformly charged outer surface to facilitate the adsorption of HgTe NCs. The outer layer was PAH, therefore providing a positively charged surface for adsorption of the HgTe NCs. Each HgTe NC adsorption step was followed by the deposition of a PE_3 film to regenerate a uniform surface charge prior to the next HgTe NC adsorption step.

TEM confirmed the formation of PE/HgTe NC multilayers on colloidal spheres. Figure 1a shows a TEM micrograph of a 640-nm PS sphere coated with a $(PE_3$/HgTe$)_2$ multilayer film and capped with an additional PAH/PSS bilayer film (PE_2) [PS−$(PE_3$/HgTe NC$)_2$/PE_2]. The outermost PE_2 film is of significant importance in the formation of the colloidal crystals (see below). The HgTe NCs in the coating can be seen because they have a higher electron contrast than the PEs. High-resolution TEM allows visualization of single HgTe NCs in the composite multilayer shell on the PS spheres, clearly showing resolved lattice planes of single crystalline particles (Figure 1a inset). The diameters of the PS spheres coated with different numbers of HgTe NC layers are about 660 nm for PS−$(PE_3$/HgTe NC$)_1$/PE_2, 675 nm for PS−$(PE_3$/HgTe NC$)_2$/PE_2, and 690 nm for PS−$(PE_3$/HgTe NC$)_3$/PE_2. This highlights that the thickness of the nanocomposite multilayer shell can be controlled by varying the number of layers deposited: the PE_3/HgTe NC film thickness is about 8−10 nm.

The nanocomposite multilayers, $(PE_3$/HgTe NC$)_n$/PE_2, on the PS spheres form a smooth film. The resulting core−shell spheres should therefore behave similarly to uncoated particles and form ordered colloidal crystals when allowed to sediment under controlled drying conditions. We found that, if the HgTe NCs formed the outermost layer on the PS spheres, it was difficult to prepare colloidal crystals with long-range order. This was overcome by the deposition of an additional PAH/PSS bilayer film on the PS−$(PE_3$/HgTe NC$)_n$ spheres, in agreement with our recent work on the crystallization of spheres coated with PE/gold nanoparticle multilayers, where PE coatings with outermost PE layers were found to be essential for forming crystals.[24] Having PSS as the outermost layer was also necessary for the formation of colloidal crystal films on the quartz slides because of the negatively charged quartz surface. Figure 1b shows a typical SEM micrograph of a colloidal crystal film formed from PS−$(PE_3$/HgTe NC$)_2$/PE_2 spheres on hydrophilic quartz slides. The structure of the resulting colloidal crystal is identical to that obtained with

(21) Caruso, F.; Lichtenfeld, H.; Donath, E.; Möhwald, H. *Macromolecules* **1999**, *32*, 2317.
(22) Denkov, N. D.; Velev, O. D.; Kralchevsky, P. A.; Ivanov, I. B.; Yoshimura, H.; Nagayama, K. *Langmuir* **1992**, *8*, 3183.
(23) Rogach, A. L.; Koktysh, D. S.; Harrison, M.; Kotov, N. A. *Chem. Mater.* **2000**, *12*, 1526.
(24) Liang, Z.; Susha, A. S.; Caruso, F. *Adv. Mater.* **2002**, *14*, 1160.

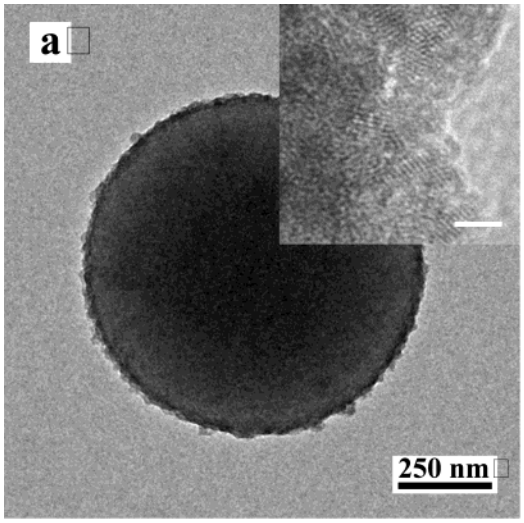

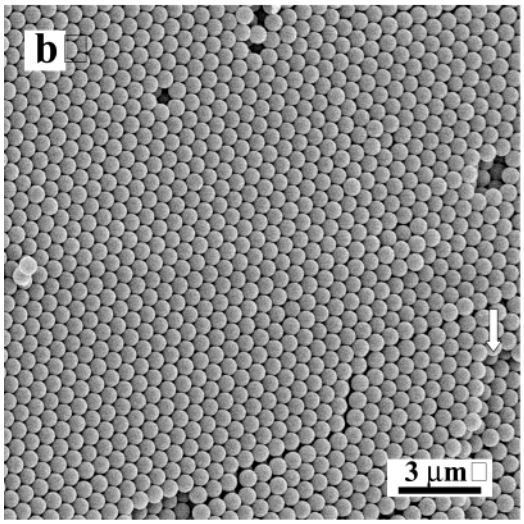

Figure 1. (a) TEM micrograph of a PS sphere coated with a $(PE_3/HgTe\ NC)_2/PE_2$ nanocomposite multilayer film. A high-resolution TEM image is shown in the inset. The scale bar in the inset corresponds to 5 nm. (b) SEM micrograph of a colloidal crystal made from PS spheres coated with a $(PE_3/HgTe\ NC)_2/PE_2$ nanocomposite multilayer film. The PS spheres used are 640 nm in diameter. The HgTe nanocrystals are 3.5 nm in size. The white arrow indicates the (110) plane of the fcc structure of the colloidal crystal.

uncoated particles. The (111) plane of the face-centered-cubic (fcc) structure is formed along the direction perpendicular to the quartz slide surface, and square arrays of bcc structure are observed occasionally in the interstices between hexagonally packed domains. The view of the resulting colloidal crystals through crack domains, indicated by an arrow in Figure 1b, shows (110) planes of fcc structures, revealing the 3D nature of the colloidal crystal film.

Figure 2 shows a typical near-infrared (NIR) reflectance spectrum from colloidal crystals formed from $PS-(PE_3/HgTe\ NC)_2/PE_2$ spheres. The specular reflectivity peak, so-called stop band, is clearly visible, which is due to reflection of the incident light by the resulting $PS-(PE_3/HgTe\ NC)_2/PE_2$ colloidal crystal. The Fabry−Perot fringes, indicated by the arrows in Figure 2, are due to the interference between the reflection of light from the top and bottom surfaces of the samples. The prominent

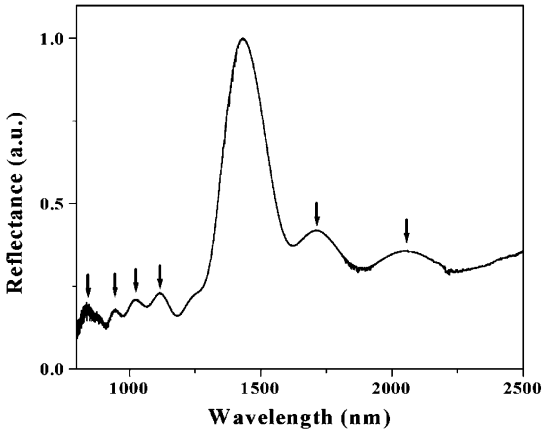

Figure 2. Near-infrared reflectance spectrum of the colloidal crystal formed from $PS-(PE_3/HgTe\ NC)_2/PE_2$ spheres. The spectrum was recorded at an angle of incidence of 12°. The arrows indicate the Fabry−Perot fringes.

feature in the data is that the observed stop bands red shift with the number of $PE_3/HgTE$ NC layers deposited. The stop band of the bare PS colloidal crystal occurs at 1345 nm (not shown), whereas the stop bands of colloidal crystals of the PS spheres coated with one, two, and three $PE_3/HgTe$ NC layers are located at 1425, 1435, and 1460 nm, respectively. Using colloidal crystals made from uncoated PS spheres as a reference, the largest red shift (from 1345 to 1425 nm) was observed for the deposition of $PE_3/HgTe/PE_2$ multilayers on the PS spheres. This is attributed to the increase in both the diameter and the effective refractive index of the prepared coated spheres, according to the Bragg equation.[25] The smaller relative changes for the higher layer numbers ($n = 2$ and 3) can be attributed to variations in the HgTe NC loadings and the thicknesses of the coatings. Assuming that a HgTe NC monolayer is formed on the PS spheres, the layer thickness is equal to the size of the HgTe NCs, 3.5 nm. The PE (either PAH or PSS) monolayer thickness is 1.5 nm;[21] hence, the HgTe NC volume fractions for the $PS-(PE_3/HgTe\ NC)PE_2$, $PS-(PE_3/HgTe\ NC)_2PE_2$, and $PS-(PE_3/HgTe\ NC)_3PE_2$ spheres can be calculated to be 3, 6, and 8%, respectively. Considering the low volume fractions of HgTe NCs in the coated spheres, the red shift of the stop band with increasing coating thickness (i.e., number of layers) on the PS spheres is dominated mainly by the size change of the coated spheres, largely caused by the PE coatings. Our previous work showed that the optical stop band of colloidal crystals made of PS spheres coated with PE multilayers could be red shifted by about 50 nm for an eight-layer PAH/PSS coating.[24]

The HgTe NCs used here have a strong emission in the region of 1000−1500 nm, which overlaps with the stop bands of the prepared composite $PS-(PE_3/HgTe\ NC)_nPE_2$ colloidal crystals. Photoluminescence (PL) measurements show that the stop bands of the $PS-(PE_3/HgTe\ NC)_nPE_2$ colloidal crystals suppress the emission of the HgTe NCs. In the case of using the transmission mode to detect PL, the emission of the

(25) $\lambda = 2(^2/_3)^{1/2}D(n^2 - \sin\theta)^{1/2}$, where λ is the wavelength of the stop band of the colloidal crystals, D is the diameter of the spheres, n is the effective refractive index, and θ is the incident angle. See, for example: Flaugh, P. L.; O'Donnell, S. E.; Asher, S. A. *Appl. Spectrosc.* **1984**, *38*, 847.

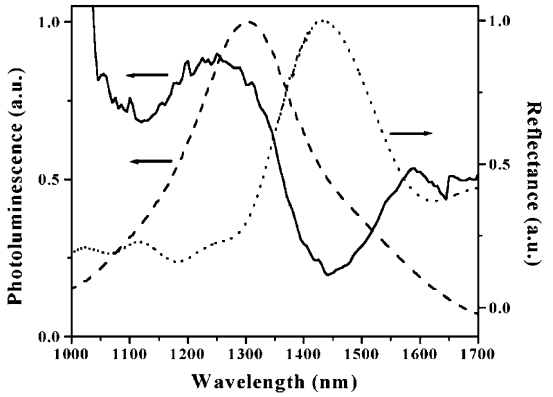

Figure 3. Photoluminescence spectra of the PS−$(PE_3/HgTe\ NC)_2/PE_2$ colloidal crystals collected at 90° with respect to the excitation light beam (scattering mode, dashed curve) and from the back side of the samples (transmission mode, solid curve). The excitation wavelength was 514 nm, and the excitation density was kept very low (0.05 mW cm^{-2}, to excite only the NCs in the bottom layers of the colloidal crystal). The dotted curve indicates the stop band of PS−$(PE_3/HgTe\ NC)_2/PE_2$ colloidal crystals recorded at the angle of incidence of 12°.

HgTe NCs on PS spheres forming PS−$(PE_3/HgTe\ NC)_2/PE_2$ colloidal crystals first penetrates through the colloidal crystals and then is collected by a detector, which allows observation of the stop band effect on the PL of the NCs. The PL spectrum of the PS−$(PE_3/HgTe\ NC)_2/PE_2$ colloidal crystal recorded by using transmission mode exhibits a dip located around 1450 nm (Figure 3, solid line). Considering that the PS−$(PE_3/HgTe\ NC)_2/PE_2$ colloidal crystal has a stop band located at 1435 nm at an incident angle of 12° (Figure 3, dotted line), a stop band of 1453 nm at the incident angle of 0° (normal transmission or reflection) can be calculated from the Bragg equation.[25] Therefore, the emission dip (1450 nm) in the PL spectrum of the PS−$(PE_3/HgTe\ NC)_2/PE_2$ colloidal crystal is close to the reflectance maximum of the PS−$(PE_3/HgTe\ NC)_2/PE_2$ colloidal crystal (1453 nm), which demonstrates modification of the emission of the HgTe NCs deposited on the PS spheres by the stop band of the PS−$(PE_3/HgTe\ NC)_2/PE_2$ colloidal crystals. In contrast, in the case of using the scattering mode to detect the PL, the emission collected by the detector comes mostly from the HgTe NCs on the top surface of the colloidal crystals, so the stop band of the resulting colloidal crystal (Figure 3, dotted line) has little influence on the resulting spectra (Figure 3, dashed line).

Importantly, our method of embedding light-emitting species into colloidal crystals utilizing colloidal spheres coated with nanoparticles (either HgTe as shown here or CdTe[18]) and PEs allows us to preserve the luminescent properties of the NCs. By impregnation of the voids of colloidal crystals with NCs from solution,[8a] the NC luminescence is either quenched or strongly changed by interactions between the closely packed NCs. By incorporation of NCs into the silica spheres through a multistep silanization procedure,[14e] the luminescence of the NCs becomes sufficiently weakened as well.

Composite Inverse Opals Prepared by Utilizing PS−$(PE_3/NC)_n/PE_2$ Colloidal Crystals as Templates. The PS−$(PE_3/NC)_n/PE_2$ colloidal crystals were used to template the formation of TiO_2 inverse opals. An IPA solution of TIP was infiltrated into the colloidal crystals, and following solidification of TIP and calcination, composite inverse opal films were obtained. However, the use of PS−$(PE_3/HgTe\ NC)_n/PE_2$ spheres for inverse opal formation is different from the use of uncoated spheres[8,9] or those coated with pure PE multilayer films:[26] NCs deposited on spheres cannot be removed in the calcination process. As a result, when using PS−$(PE_3/NC)_n/PE_2$ colloidal crystals as templates to form TiO_2 inverse opals, removal of the organic materials (PS sphere and PE multilayers) by calcination leaves behind not only a 3D highly ordered interconnected macroporous TiO_2 scaffold but also NCs (that might be fused to form a layer, bulklike or nanocrystalline, depending on the nature of the NCs used and the calcination temperature) embedded in the interior surface of the resulting scaffold. Figure 4a shows typical SEM micrographs of the composite TiO_2 inverse opals formed by templating PS−$(PE_3/HgTe\ NC)_2/PE_2$ colloidal crystals. The cracked regions of the samples exhibit

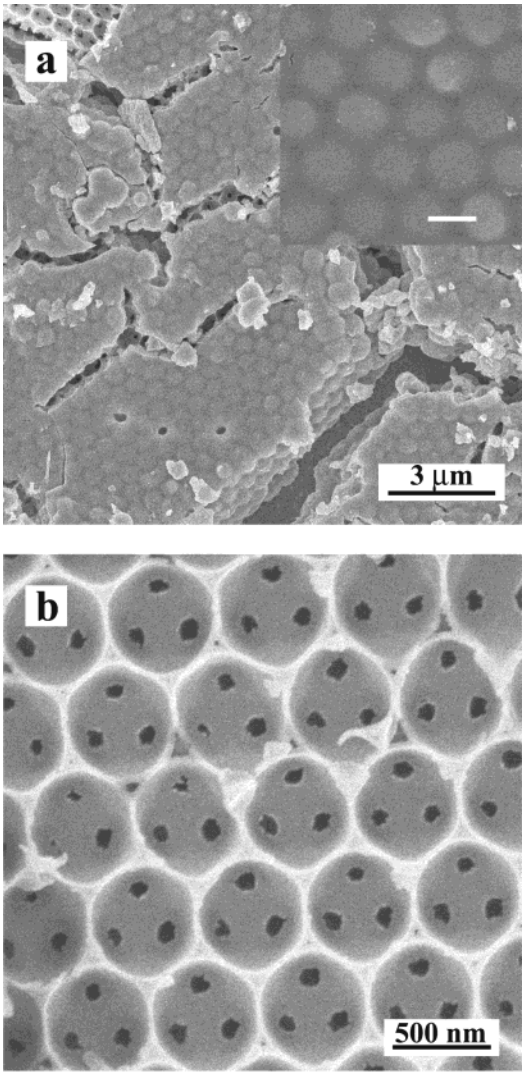

Figure 4. (a) SEM micrographs of the TiO_2/HgTe inverse opals formed by using PS−$(PE_3/HgTe\ NC)_2/PE_2$ colloidal crystals as templates. The PS spheres used are 640 nm in diameter, and the HgTe nanocrystals are 3.5 nm in size. The inset in a shows a high-magnification image of the top surface of the prepared samples. The scale bar in the inset corresponds to 500 nm. (b) High-magnification SEM image taken from a broken area of the TiO_2/HgTe inverse opal.

(26) Wang, D.; Caruso, F. *Adv. Mater.* **2003**, *15*, 205.

ordering in the vertical direction, which reveals that the crystal structure in the resulting film is fcc, similar to that obtained for the PS−$(PE_3$/HgTe NC$)_2/PE_2$ colloidal crystals (Figure 1b). The closed pore structure on the top surface of the inverse opal film is likely due to a certain amount of the TIP solution being adsorbed by the PE multilayer films at the interfacial regions between the samples and the quartz slides, although it was difficult to infiltrate these regions well.[27] Highly ordered macroporous structures are seen at the broken regions (Figure 4a). SEM reveals pores, interconnected by channels, at higher magnification (Figure 4b), which confirms a 3D inverse opal structure. Energy-disperse X-ray (EDX) analysis indicates the presence of Ti, O, Hg, and Te (not shown), demonstrating the presence of HgTe in the inverse opals after calcination; specifically, TiO_2/HgTe composite inverse opals have been constructed. It is rather unlikely that HgTe in this structure remains in the form of NCs, as the organic stabilizing shells on the NCs would not withstand heating at 500 °C under oxygen. It is also possible that some of HgTe oxidized into HgO, or TeO, or even $HgTeO_3$. The center-to-center distance of the resulting TiO_2/HgTe inverse opals is 600 ± 10 nm, corresponding to a shrinkage of 18%. The wall thickness is 40 ± 5 nm, and the diameter of the circular channels is 95 ± 10 nm. This approach provides a simple and versatile means that enables tailoring of the functionality of the resulting composite inverse opals, depending on the coating materials.

(27) Wang, D.; Caruso, R. A.; Caruso, F. *Chem. Mater.* **2001**, *13*, 364.

Conclusions

A series of multilayer films consisting of HgTe NCs and PEs were coated onto PS colloidal spheres, and it was demonstrated that these coated spheres could be crystallized to form composite colloidal crystals. Increasing the number of NC layers deposited on the spheres leads to an increase in both the diameter and the effective refractive index of the composite spheres, which causes a red shift of the stop bands of the prepared composite colloidal crystals. In the case of colloidal crystals made from PS−$(PE_3$/HgTe NC$)_nPE_2$, PL experiments demonstrated the possibility of modifying the emission of the HgTe NCs deposited on spheres by the stop band of the PS−$(PE_3$/HgTe NC$)_nPE_2$ colloidal crystals. By infiltrating a TiO_2 precursor solution into the composite colloidal crystals, composite inverse opals of TiO_2/HgTe were constructed, with HgTe embedded in the interior surface of the macroporous TiO_2.

Acknowledgment. R. Wehrspohn, J. Heitmann, and J. Schilling from the Max Planck Institute of Microstructure Physics are thanked for assistance with the optical measurements. D. Wang acknowledges the Alexander von Humboldt Foundation for a research fellowship. This work was financially supported by the BMBF and by the DFG "Photonic Crystals" program.

CM031003O